

Stability investigation of a cryo soft x-ray microscope by fiber interferometry

Cite as: Rev. Sci. Instrum. **91**, 023701 (2020); <https://doi.org/10.1063/1.5138369>

Submitted: 14 November 2019 . Accepted: 09 January 2020 . Published Online: 03 February 2020

M. Kördel , K. G. Y. Arsana , H. M. Hertz , and U. Vogt 



View Online



Export Citation



CrossMark

ARTICLES YOU MAY BE INTERESTED IN

[Apparatus design for measuring of the strain dependence of the Seebeck coefficient of single crystals](#)

Review of Scientific Instruments **91**, 023902 (2020); <https://doi.org/10.1063/1.5127530>

[SquidLab—A user-friendly program for background subtraction and fitting of magnetization data](#)

Review of Scientific Instruments **91**, 023901 (2020); <https://doi.org/10.1063/1.5137820>

[Optimization analysis of piezoelectric actuator based on energy transfer](#)

Review of Scientific Instruments **91**, 025001 (2020); <https://doi.org/10.1063/1.5127165>



VACUUM SOLUTIONS FROM A SINGLE SOURCE

Pfeiffer Vacuum stands for innovative and custom vacuum solutions worldwide, technological perfection, competent advice and reliable service.

[Learn more!](#)

Stability investigation of a cryo soft x-ray microscope by fiber interferometry

Cite as: Rev. Sci. Instrum. 91, 023701 (2020); doi: 10.1063/1.5138369

Submitted: 14 November 2019 • Accepted: 9 January 2020 •

Published Online: 3 February 2020



M. Kördel,^{a)}  K. G. Y. Arsana,^{b)}  H. M. Hertz,^{b)}  and U. Vogt^{b)} 

AFFILIATIONS

KTH Royal Institute of Technology, Department of Applied Physics, Biomedical and X-ray Physics, Albanova University Center, 106 91 Stockholm, Sweden

^{a)} Author to whom correspondence should be addressed: mikael.kordel@biox.kth.se

^{b)} Electronic mail: uvogt@kth.se

ABSTRACT

We present a stability investigation of the Stockholm laboratory cryo soft x-ray microscope. The microscope operates at a wavelength of 2.48 nm and can image biological samples at liquid-nitrogen temperatures in order to mitigate radiation damage. We measured the stability of the two most critical components, sample holder and optics holder, *in vacuo* and at cryo temperatures at both short and long time scales with a fiber interferometer. Results revealed vibrations in the kHz range, originating mainly from a turbo pump, as well as long term drifts in connection with temperature fluctuations. With improvements in the microscope, earlier stability issues vanished and close-to diffraction-limited imaging could be achieved. Moreover, our investigation shows that fiber interferometers are a powerful tool in order to investigate position-sensitive setups at the nanometer level.

© 2020 Author(s). All article content, except where otherwise noted, is licensed under a Creative Commons Attribution (CC BY) license (<http://creativecommons.org/licenses/by/4.0/>). <https://doi.org/10.1063/1.5138369>

I. INTRODUCTION

Soft x-ray microscopy provides a unique tool to study a wide range of samples with high resolution and contrast under relatively unperturbed conditions. The absorption and scattering properties of x rays enable nanometer-scale resolution, even in thick objects ($>1 \mu\text{m}$), making them a suitable choice for tomographic (3D) imaging.¹ Biological samples such as whole cells are especially suited for x-ray microscopy in the water-window ($\lambda \approx 2.3\text{--}4.4 \text{ nm}$ and $E = 284\text{--}540 \text{ eV}$) due to the natural high contrast between carbon-rich and oxygen-rich materials. These samples are preferably kept in their native hydrated state and cryofixed prior to imaging. As a comparison, electron microscopy (EM) can provide higher resolution but lack the sufficient penetration capabilities. Furthermore, this technique requires extensive sample preparation that often entails physical and chemical alterations to the sample and its environment. Super-resolution optical methods such as STED and PALM² have emerged as candidates for tomographic imaging of thick objects with high resolution. However, the contrast relies completely on fluorescent dyes, attaching to certain objects in the sample, thus requiring prior knowledge about the features one would like to see.

Modern soft x-ray microscopes typically rely on the high spectral brightness produced at synchrotrons. These microscopes have proven highly useful for a range of different imaging applications.^{1,3–5} However, the large footprint and corresponding cost of such facilities have a negative impact on the accessibility to the broader science community. Laboratory-source based microscopes are being developed as a complement to the synchrotron-based instruments with comparable, although typically less versatile, capabilities.^{6,7} Common for all instruments is that they rely on high stability between sample and imaging components in order to achieve nanometer-scale resolution.⁸ This includes resistance to ambient noise, vibrations, and drift that most often exist in the lab environment. Instruments that keep the sample or other sensitive components at cryogenic temperatures are especially at risk of being affected by thermal drift or vibrations from liquid nitrogen or other cryogens.

Here, we present stability measurements on the Stockholm laboratory x-ray microscope, which is based on a compact liquid-nitrogen-jet laser-plasma source and operates in the water window at $\lambda = 2.48 \text{ nm}$. This microscope has previously not been able to achieve diffraction-limited resolution, set by the zone plate (ZP)

objective. Chromatic aberrations, astigmatic zone plates, and photon noise due to limited source brightness have been discussed as possible reasons. However, we show here that the main limiting factor has been high frequency vibrations in optics and sample holders. Detailed displacement measurements were performed using a vacuum compatible interferometric displacement sensor, and real-time frequency analysis was used to identify sources of vibrations. Furthermore, effects of liquid nitrogen in the microscope setup were measured and shown to have a negative impact on the imaging resolution, if not properly handled. These results are of general interest for any position-sensitive setups at the nanometer level and especially any setups containing cryogenic liquids.

II. EXPERIMENTAL ARRANGEMENT

A. Laboratory cryo soft x-ray microscopy

The Stockholm Laboratory x-ray microscope,⁹ shown in Fig. 1, utilizes the $\lambda = 2.48$ nm line emission from a nitrogen plasma, generated by focusing a beam of $\lambda = 1064$ nm, 600 ps Nd:YAG slab laser (Fraunhofer ILT, Aachen)¹⁰ onto a liquid nitrogen jet at average powers up to ~ 100 W. The jet is created by letting high purity gaseous nitrogen pass through a liquid-nitrogen cooled cryostat, which is mounted on top of the microscope setup. The gas pressure drives the liquefied nitrogen through a $30\ \mu\text{m}$ diameter glass capillary into the vacuum chamber where it meets the laser focus.

The $\lambda = 2.48$ nm line emission from the plasma is collected and imaged onto the sample plane by using a normal-incidence multilayer condenser mirror (MLM), which thereby works as a monochromator. A 30 nm outer zone width Ni zone plate (ZP), placed on a small aluminum cone, is used to image the sample onto a CCD detector with $2048 \times 2048\ 13.5\ \mu\text{m}$ pixels. In order to prevent the non-diffracted light from the zone plate from reaching the detector, a central stop (CS) blocks parts of the x-ray beam to create a hollow-cone illumination.

Due to the absorption properties of the soft x rays in air, all of this takes place in vacuum of about 10^{-3} – 10^{-6} mbar. Pumping is done from two sides of the microscope using a rough pump and a

turbo pump at either side. The rough pumps can be placed several meters away to avoid vibrations, but the turbo pumps have to be placed in close connection with the microscope and are mounted on the same optical table. Models using magnetic bearing systems (TMH 1000 MC and TMH 071 P, Pfeiffer) were specifically selected for low-noise and low-vibration operation.

The sample stage used in the microscope is a modified TEM goniometer stage (FEI), which allows movement in all directions including rotation for tomography. The sample itself is mounted on a specialized sample holder with a 23 cm long stick, which can be inserted in the microscope during operation through a vacuum sluice. Cryofixed samples require a temperature regulated cryo sample holder (Gatan), filled from the outside with liquid nitrogen. This is the sample holder shown in Fig. 1. However, for wet and dry samples at room temperature, a sample stick of more simple design is used.

A theoretical limit for the attainable resolution of zone plate based full-field microscopes is set by the outer zone width, Δr , and the Rayleigh resolution criterion,¹¹

$$1 \text{ full period} = \frac{1.22\Delta r}{\lambda}. \quad (1)$$

For a zone plate with 30 nm outermost zone width, this means an attainable resolution of 37 nm full period or 18 nm half period. Before the stability investigation, presented here, a maximum half-period resolution of about 35 nm could be achieved.

B. Interferometric displacement measurements

Fiber-optic based interferometry is a technique widely utilized in industry and research due to its nanometer to picometer accuracy.¹² In the present paper, we used a fiber-optic based displacement measuring interferometer (IDS3010, Attocube) to analyze the stability of the Stockholm laboratory cryo x-ray microscope over a wide range of time scales. An overview of the experimental arrangement (Fig. 1) shows the fiber-coupled sensor head mounted inside the vacuum of the microscope, about 10 cm away from the target. This device employs the Fabry–Perot Interferometer (FPI) operating principle, where a reference beam is created by a reflection at the

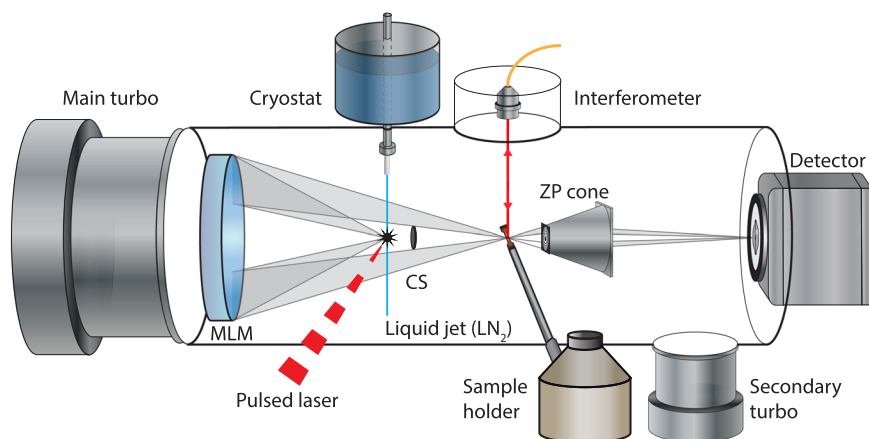


FIG. 1. Stability measurement setup in the Stockholm laboratory x-ray cryo microscope. The interferometric sensor head, used for the displacement measurements, was mounted inside the vacuum of the microscope, directly above the sample (shown here) or the zone plate cone. Two turbo pumps can be seen directly connected to the vacuum chamber.

uncoated end of the fiber. The transmitted light travels to the target and reflects back into the sensor head, where it superimposes with the reference.¹²

The IDS3010 comes with various sensor heads that can be chosen based on the experimental setup. The M12/F40 sensor head was used due to its compact physical dimensions and wide of range working distances on high reflective targets (20–1100 mm), which suited the limited space in the microscope's vacuum chamber. This sensor head was mounted onto a mirror holder (MK05, Thorlabs), which was clamped tightly to the microscope chamber by CF-flanges. The mirror holder setup was shown to provide robust and accurate alignment, needed to get a high and constant reflected signal from the targets.

In the investigation of fast vibrations, the sample holder and the zone plate cone were used as targets. They were suspected to transmit vibrations induced by adjacent instruments or the noisy laboratory environment and thereby affect the attainable resolution. We note that the source and condenser optic can only influence the illumination distribution in the images, but not the image position. The detector, on the other hand, could in theory affect the resolution but is considerably less sensitive to vibrations due to the high magnification used ($M \approx 1000$).

A gold coated standard silicon nitride (Si_3N_4) membrane window (Silson) was mounted on the sample holder and used as a target for the $\lambda = 1520$ nm laser from the interferometer. Thereby, the vibration measurements on the sample holder were done with conditions identical to actual microscope operation. Measurements on the zone plate cone were more challenging because the cone shape made the optical alignment very difficult. Instead, a new zone plate cone was made with the same material and dimensions, but with a polished flat surface facing the sensor head. This target was assumed to have similar vibration properties, especially since all parts up to the zone plate cone, including base plates and a linear motor, remained unchanged.

Displacement measurements involving liquid nitrogen in the cryo sample holder and the cryostat were done on both short and long time scales. Fast vibrations were suspected to be induced by movements, such as bubbling, in the cryogenic liquid, while slow drifts typically arise as the temperature changes. For this reason, the cryo sample holder is temperature controlled and kept at a fixed temperature between -165°C and -170°C during imaging. However, the actual effects of the temperature control have previously not been measured.

All displacement data acquisition was done using a commercially supplied software (WAVE, Attocube). This software also provides real-time fast Fourier transform (FFT) of the displacement data for easy vibration spectrum analysis. Prior to data acquisition, an alignment interface is used to optimize the reflection from the target and thus the contrast of the measured interference. A contrast of $>500\%$ is recommended for accurate measurements. The alignment was done by first adjusting the sensor head in its mirror holder setup. In the next step, the vacuum chamber was closed and pumped. The final alignment for measurements on the sample holders was done using the degrees of freedom provided by the sample stage, which includes fine movements in all directions and rotation steps of down to 0.01° around one axis. The measurement on the modified zone plate cone did not require additional alignment after pumping the vacuum chamber.

III. RESULTS AND DISCUSSION

A. Fast vibration analysis

The results of displacement measurements on the dry sample holder and the zone plate cone are shown in Figs. 2 and 3, respectively. The measurements on both targets are performed within 10 s to imitate a typical imaging exposure time. As a merit value for the vibration amplitude in the time domain, we use two standard deviations (2σ) from the mean displacement. This value is estimated to be comparable to the vibration limited (half-period) resolution, and furthermore, it corresponds well to the perceived width of the plots.

Figures 2(a)–2(d) show the displacement data from the dry sample holder in the time domain. The corresponding spectra, in the frequency domain, are displayed to the right of each displacement plot, i.e., in Figs. 2(e)–2(h). The first two measurements were done with the main turbo pump turned on and off, respectively. The resulting vibration amplitudes (2σ) were 26 nm [Fig. 2(a)] and 4 nm [Fig. 2(b)]. Due to the significant difference, the main turbo pump was readily recognized as a key source of vibrations, even though low-vibration operation is stated in the technical specifications. This conclusion was further established by considering the corresponding vibration frequency spectra. A strong peak at 660 Hz, exactly matching the rotation frequency of the turbo pump, is presented in Fig. 2(e), as well as side peaks at 330 Hz and 1320 Hz, corresponding to half and double the rotation frequency. All these peaks completely disappear in Fig. 2(f), where the pump has been turned off.

The vibrations could be somewhat reduced by modifications to the sample stage chamber, making the construction more rigid. However, with the main turbo pump directly connected to the main chamber, the high-frequency (>100 Hz) vibrations could not be removed. At this point, removing the source of the vibrations became necessary. This could be done by inserting a vibration dampening bellow (Pfeiffer) between the main turbo pump and the vacuum chamber, and mounting the turbo pump on a separate table, thus effectively decoupling it from the microscope.

Displacement measurements on the dry sample holder were repeated after implementing the modifications to the setup, and the results are shown in Figs. 2(c) and 2(d). The amplitude of the vibrations was at this point <6 nm, both with the turbo pump turned on [Fig. 2(c)] and off [Fig. 2(d)]. The corresponding vibration frequency spectra, shown in Figs. 2(g) and 2(h), confirm that the 660 Hz frequency, and the side peaks at 330 Hz and 1320 Hz were completely removed. Some small peaks at low frequencies (<200 Hz) in all FFT plots [Figs. 2(e)–2(h)] indicate that additional sources contribute to the vibrations of the sample holder. Further measurement showed that these additional sources include ambient sound, a 20-Hz repetition rate laser, and flow of cooling water to various components in the setup. However, the amplitude of these vibrations is well within the acceptable range considering the diffraction limit of about 18 nm half-period [Eq. (1)]. Therefore, these results are not further discussed here.

In parallel with the displacement measurements on the dry sample holder, we performed the same measurements on the zone plate cone. The results are shown in Fig. 3. The amplitude of the vibrations before implementing the modifications to the setup was 15 nm with the turbo pump turned on [Fig. 3(a)] and 3 nm with the turbo pump turned off [Fig. 3(b)]. We note that these values

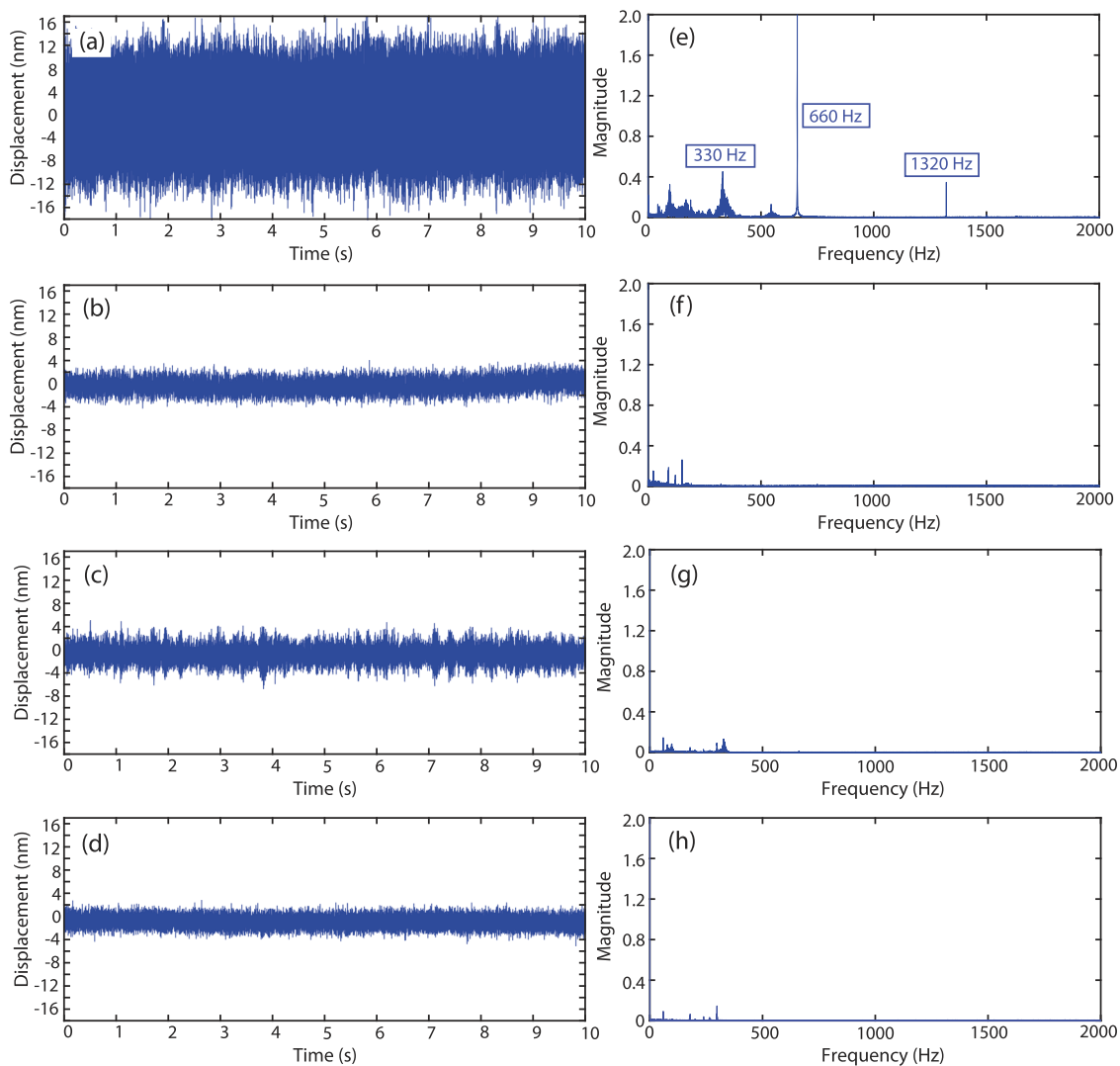


FIG. 2. Stability measurements on the dry sample holder. The displacement plots in the time domain are shown in the left column, and the corresponding spectra in the frequency domain are shown to the right. Four separate measurements are presented: With the main turbo pump connected to the microscope chamber and turned on [(a) and (e)] and off [(b) and (f)]. With the main turbo pump decoupled from the microscope chamber and turned on [(c) and (g)] and off [(d) and (h)].

are lower than for the dry sample holder, but likely big enough to affect the imaging resolution. After decoupling the main turbo pump, vibration amplitude was about 3 nm with the pump turned on [Fig. 3(c)] as well as off [Fig. 3(d)].

The corresponding vibration frequency spectra [Figs. 3(e)–3(h)] show two distinct differences from the measurements on the dry sample holder. In Fig. 3(e), we can only distinguish the 660 Hz peak, but no side peaks. Furthermore, we see no low-frequency peaks with the pump turned off or after decoupling it from the main chamber [Figs. 3(f)–3(h)]. Both differences are probably due to a more rigid setup holding the zone plate and due to the fact that the zone plate cone has no direct contact with the outside and its ambient sounds.

B. Total relative vibrations of imaging components

A control experiment was designed to make sure that displacement of the sensor head did not contribute significantly to the measurement results. Here, a thick aluminum plate was used as a target and mounted tightly to the main chamber wall, directly below the sensor head (cf. Fig. 1). Under these conditions, the measured displacement was due to the movement of the sensor head relative to the chamber. With the main turbo pump still rigidly connected to the microscope, the measured vibration amplitude was 5 nm. This is significantly less than 30 nm and 15 nm for the sample holder [Fig. 2(a)] and zone plate cone [Fig. 3(a)], respectively.

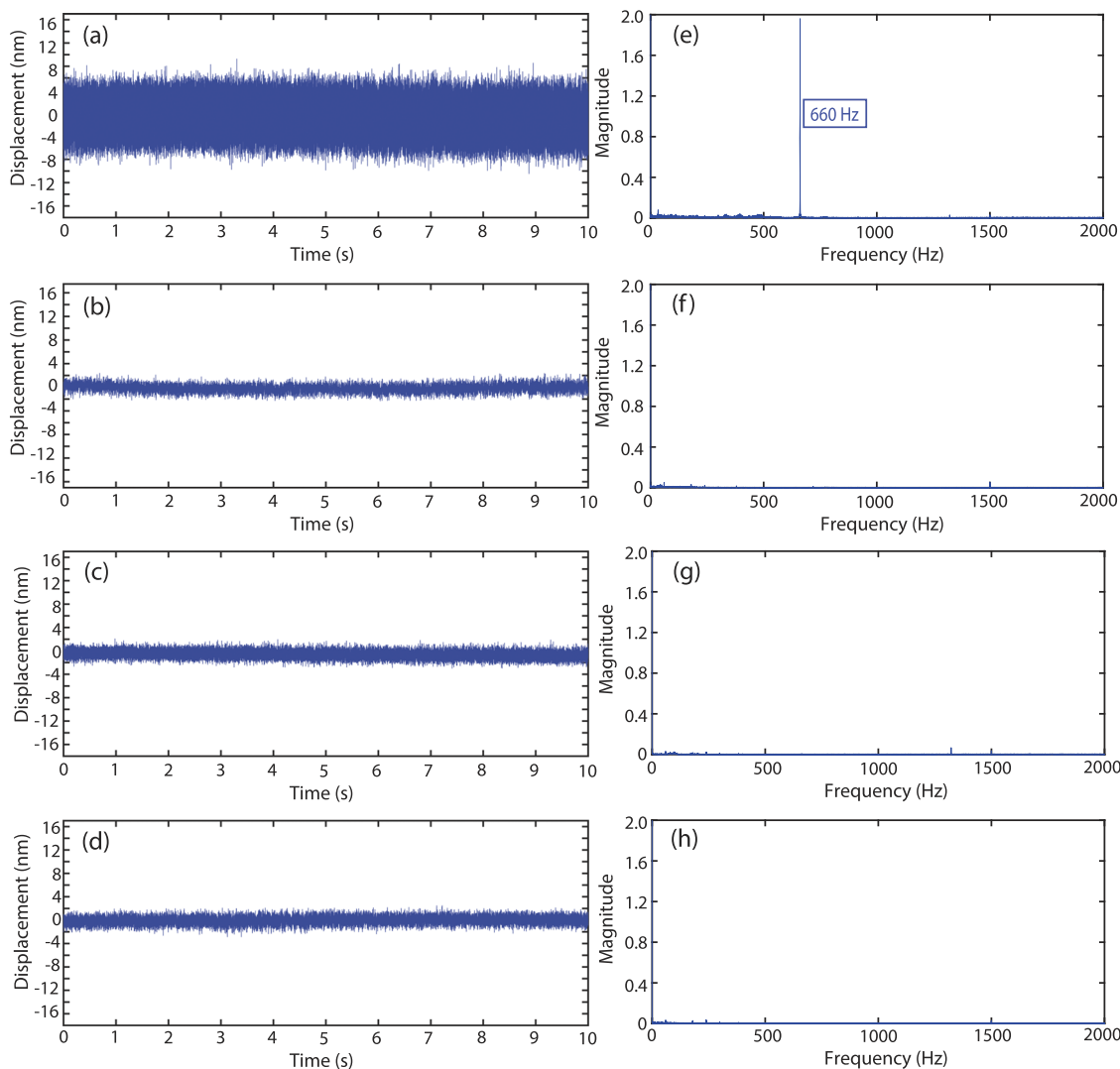


FIG. 3. Stability measurements on the zone plate cone. The displacement plots in the time domain are shown in the left column, and the corresponding spectra in the frequency domain are shown to the right. Four separate measurements are presented: With the main turbo pump connected to the microscope chamber and turned on [(a) and (e)] and off [(b) and (f)]. With the main turbo pump decoupled from the microscope chamber and turned on [(c) and (g)] and off [(d) and (h)].

This result could also be used to estimate the total relative vibrations between the sample and the zone plate objective. Assuming that all displacements are normally distributed, the total relative displacement of two independent components will also be normally distributed. Furthermore, the standard deviation squared will be equal to the sum of the individual standard deviations squared. Using this method, the sensor head vibrations were subtracted from the measurements on the sample holder and zone plate. After that, the vibration amplitudes of the sample holder and the zone plate were added, giving their total relative vibrations. The result before the modifications to the microscope setup was 30 nm, which is clearly in the same order of magnitude as the achievable resolution. After the vibration damping modifications, the total relative vibration amplitude was only 5 nm.

C. Effects of liquid nitrogen

Liquid nitrogen is commonly used in x-ray microscopy and cryo EM to keep the sample under cryogenic conditions during imaging. As described in Sec. II A, the Stockholm laboratory x-ray microscope uses a temperature controlled cryo sample holder (Gatan), which is cooled by filling it with liquid nitrogen. The sample holder has to be refilled a few times during each imaging experiment, which lasts about 2 h. Furthermore, liquid nitrogen is used to cool the cryostat, which in turn delivers the liquid nitrogen jet for the laser-plasma x-ray source.

Experience shows that any liquids close to sensitive components risk inducing vibrations. Furthermore, any changes in temperature might induce drifts. Therefore, both short-term and

long-term displacement measurements, performed under actual cryo-imaging conditions, are necessary for a full assessment of the stability of the microscope. All displacement measurements under cryo conditions were performed after putting in the vibration dampening bellow between the main turbo pump and the microscope chamber.

Figure 4 summarizes the effects of liquid nitrogen in the microscope on a short time scale of 10 s. As a reference, a displacement measurement on the cryo sample holder at room temperature is given in Fig. 4(a). The vibration amplitude under this case was about 2 nm, which is similar to the vibrations of the dry sample holder [cf. Fig. 2(b)]. The corresponding measurement, after cooling the sample holder and keeping it at -168°C , is shown in Fig. 4(b). The amplitude of the vibrations clearly increased in this case, but stayed at acceptable 4 nm.

After refilling the cryo sample holder with liquid nitrogen, bubbling occurs, which was expected to have a strong impact on the stability of the sample. The effects within 10 s are shown in Fig. 4(c). Periodic bursts of a few Hz are clearly seen in the displayed data, giving an average vibration amplitude of 12 nm and peaks of about 30 nm. Similar effects were seen when filling the cryostat with liquid nitrogen [Fig. 4(d)]. Periodic bursts were attributed to bubbles forming in the not yet thermally stabilized cryostat. This created vibration pulses traveling through the setup to the sample holder, giving displacement peaks of >30 nm. The results presented in Figs. 4(c) and 4(d) indicate that thermal stabilization needs to be achieved before acquiring any high-resolution images. To further understand this, long term displacement measurements were performed on the cryo sample holder over several minutes.

Figure 5(a) shows the displacement data from the cryo sample holder at a constant temperature, a few moments after refilling the liquid nitrogen. The measurement is presented during 240 s. The large vibrations (up to 50 nm) last up for about 3 min,

before decreasing and eventually stabilizing at the acceptable levels discussed above [Fig. 4(b)]. Based on this result, we conclude that high-resolution image acquisitions can be started about 5 min after refilling the cryo sample holder with liquid nitrogen. This result will be of interest to any high-resolution cryo-imaging system, using a similar sample setup, and with exposure times in the order of seconds or more.

Similarly to the thermal stabilization of the cryo sample holder, the bubbling in the cryostat stops about 15 min after filling up the liquid nitrogen. Since the temperature stabilization of the cryostat is, in any case, necessary to start the jet for the x-ray source, there is no need to take this into further account.

Finally, we present a result showing the importance of keeping a constant temperature in the cryo sample holder. Figure 5(b) shows a displacement measurement during 240 s, where the temperature is fixed at -168.4°C for the first 160 s. The displacement up to this point was constant within <5 nm amplitude vibrations. At around 160 s, the liquid nitrogen in the sample holder had evaporated and the temperature started increasing. A close-to linear drift of 700 nm was measured over the next 80 s. At the same time, the temperature increased by only about 1°C .

D. Resolution evaluation

Concluding evidence that the improved stability had the desired effect on the resolution of the laboratory x-ray microscope was obtained by analyzing images of a gold Siemens star test target. In Fig. 6, we show three images of the same Siemens star, with a center line width of 30–35 nm, under three different conditions. Profile plots at two positions close to the center of the Siemens star provide a quantitative comparison of the attained resolution. Figure 6(a) was acquired before the stability investigation. We see that the center spokes appear smeared and cannot be completely

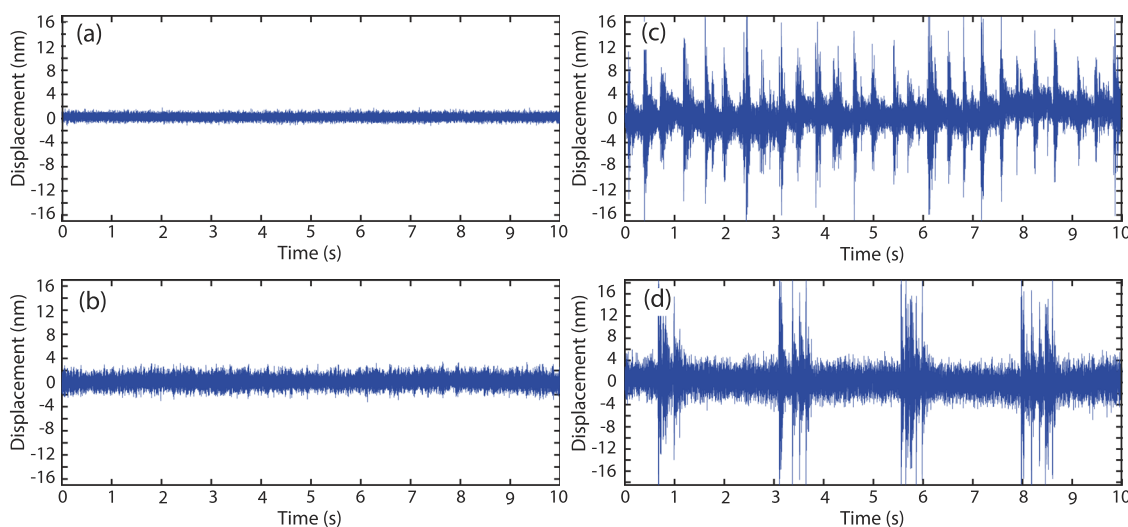


FIG. 4. Displacement measurements on the cryo sample holder under four different conditions. (a) Without liquid nitrogen, (b) >10 min after refilling the cryostat and the cryo sample holder with liquid nitrogen, (c) a few moments after refilling the cryo sample holder with liquid nitrogen, and (d) a few moments after filling the cryostat with liquid nitrogen.

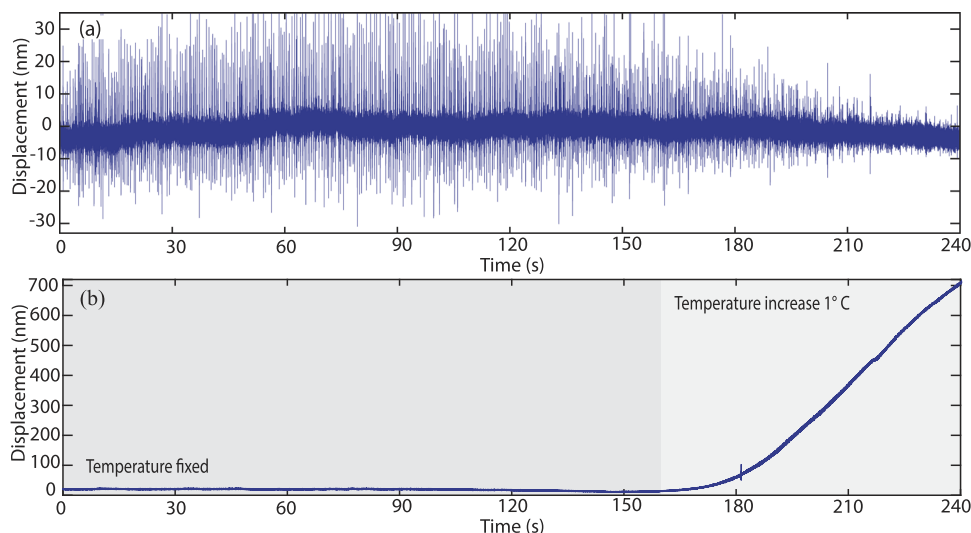


FIG. 5. Long-term displacement measurements on the cryo sample holder. Both results are presented during 240 s. (a) A large vibration amplitude caused by high evaporation of liquid nitrogen, a minute after refilling cryo sample holder. (b) Constant displacement (within <5 nm) of the cryo sample holder, kept at -168.4 °C. After 160 s, a small change in the temperature (1 °C) caused a rapid drift.

resolved. Furthermore, we see that the resolution is worse in the horizontal direction, which can be due to the vibrations of the sample holder in the vertical direction. We note that vibration of the sample along the axis of the sample stick (cf. Fig. 1) is unlikely and that horizontal vibrations (along the optical axis) would have a very little effect on the image. We estimate the resolution in this image to be 35–40 nm half period.

Figure 6(b) was acquired after the stability investigation and consequently after decoupling the main turbo pump from the microscope chamber. As expected, the reduced vibrations have a positive effect on the achieved resolution. Here, the center spokes are clearly resolved all the way to the center with appreciable improvements to the contrast. In Figs. 6(a) and 6(b), the Siemens star was mounted on the dry sample holder.

To evaluate the short-term and long-term stability under cryogenic conditions, the Siemens star was mounted on the cryo sample stick, which was then cooled by liquid nitrogen and kept at -168 °C during imaging. We emphasize that these conditions were identical to those used in imaging of cryofixed cell samples (except that the Siemens star was not submerged in liquid). The result is shown in Fig. 6(c). Once again, we see that the spokes are clearly resolved all the way to the center with a contrast equal to that in Fig. 6(b). From this result, we can conclude two things. First of all, the short-term effects of nitrogen bubbles in the cryo sample holder are negligible, as long as one waits a few minutes after refilling the liquid nitrogen [cf. Figs. 4(b), 4(d), and 5(a)]. Second, the thermal drift of the cryo sample holder is negligible due to the controlled temperature [cf. Fig. 5(b)].

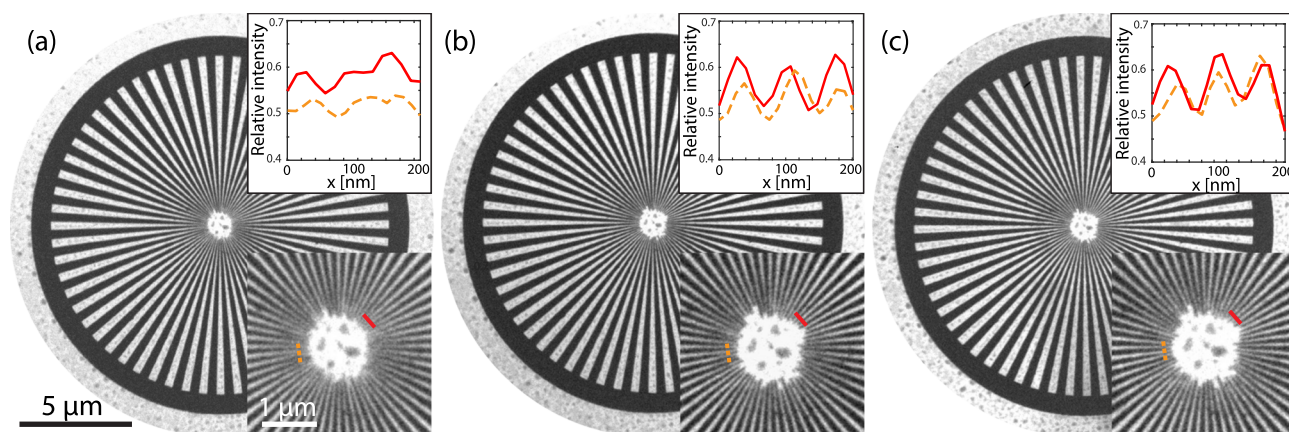


FIG. 6. Resolution comparison before and after stability investigation. (a) Laboratory x-ray microscopy of a gold Siemens star, imaged on the dry sample stick, before the stability investigation. (b) Laboratory x-ray microscopy of a gold Siemens star, imaged on the dry sample stick, after the stability investigation. (c) Laboratory x-ray microscopy of a gold Siemens star, imaged under cryo conditions (-168 °C), after the stability investigation. Profile plots at two positions close to the center of the Siemens star are included in each image to better show the improvement in resolution. The center parts of the Siemens star consist of 30–35 nm lines and spaces.

IV. CONCLUSIONS

A detailed stability investigation is important for any high-resolution imaging system. The results of this study have shown that fiber-optic based interferometry is an efficient tool for such a task, with the ability to measure displacements with nanometer accuracy in a vacuum environment. Furthermore, real-time FFT vibration analysis was shown to facilitate the identification of vibration sources.

Measurements on the Stockholm laboratory cryo soft x-ray microscope successfully identified and quantified residual vibrations in the setup. Fast vibrations with a main frequency of 660 Hz and an amplitude of 30 nm were shown to be caused by the main turbo pump, connected to the microscope vacuum chamber. A vibration dampening bellow was used to reduce the transmission of high frequency vibrations from the turbo pump to sensitive imaging components, thus limiting its relative vibrations to approximately 5 nm.

Displacement measurements on the cryo sample holder showed that the presence of liquid nitrogen can have a significant effect on the stability of the microscope. Low-frequency bursts, due to evaporation in the sample holder and the cryostat, were measured during thermal stabilization. Furthermore, small changes in the temperature of the cryo sample holder were shown to induce severe drifts. Based on these results, we were able to define experimental procedures to avoid undesirable effects of liquid nitrogen on the microscope performance.

Finally, we conclude that the reduced vibrations and controlled temperature stabilization improved the resolution of the laboratory cryo soft x-ray microscope. Close-to diffraction-limited resolution was achieved when imaging a gold Siemens star at room temperature as well as under cryo conditions. We believe that the methods presented here can be applied to a wide range of instruments with stability requirements at the nanometer level.

ACKNOWLEDGMENTS

The authors would like to thank Ulf Johansson at MAX IV for lending the interferometric displacement sensor, and Thomas Frisk and Rabia Akan for fabrication of reflective targets. This work was financed by the Swedish Research Council.

REFERENCES

- ¹M. Harkiolaki, M. C. Darrow, M. C. Spink, E. Kosior, K. Dent, and E. Duke, "Cryo-soft X-ray tomography: Using soft X-rays to explore the ultrastructure of whole cells," *Emerging Top. Life Sci.* **2**, 81–92 (2018).
- ²L. Schermelleh, A. Ferrand, T. Huser, C. Eggeling, M. Sauer, O. Biehlmaier, and G. P. Drummen, "Super-resolution microscopy demystified," *Nat. Cell Biol.* **21**, 72–84 (2019).
- ³S. Kaphishnikov, A. Weiner, E. Shimoni, P. Guttman, G. Schneider, N. Dahan-Pasternak, R. Dzikowski, L. Leiserowitz, and M. Elbaum, "Oriented nucleation of hemozoin at the digestive vacuole membrane in *Plasmodium falciparum*," *Proc. Natl. Acad. Sci. U. S. A.* **109**, 11188–11193 (2012).
- ⁴A. Cruz-Adalia, G. Ramirez-Santiago, C. Calabia-Linares, M. Torres-Torresano, L. Feo, M. Galán-Díez, E. Fernández-Ruiz, E. Pereiro, P. Guttman, M. Chiappi, G. Schneider, J. L. Carrascosa, F. J. Chichón, G. Martínez Del Hoyo, F. Sánchez-Madrid, and E. Veiga, "T cells kill bacteria captured by transinfection from dendritic cells and confer protection in mice," *Cell Host Microbe* **15**, 611–622 (2014).
- ⁵M. A. Le Gros, G. McDermott, B. P. Cinquin, E. A. Smith, M. Do, W. L. Chao, P. P. Naulleau, and C. A. Larabell, "Biological soft X-ray tomography on beamline 2.1 at the advanced light source," *J. Synchrotron Radiat.* **21**, 1370–1377 (2014).
- ⁶E. Fogelqvist, M. Kördel, V. Carannante, B. Önfelt, and H. M. Hertz, "Laboratory cryo x-ray microscopy for 3D cell imaging," *Sci. Rep.* **7**, 13433 (2017).
- ⁷H. Legall, G. Blobel, H. Stiel, W. Sandner, C. Seim, P. Takman, D. H. Martz, M. Selin, U. Vogt, H. M. Hertz, D. Esser, H. Sipma, J. Luttmann, M. Höfer, H. D. Hoffmann, S. Yulin, T. Feigl, S. Rehbein, P. Guttman, G. Schneider, U. Wiesemann, M. Wirtz, and W. Diete, "Compact x-ray microscope for the water window based on a high brightness laser plasma source," *Opt. Express* **20**, 18362 (2012).
- ⁸D. S. Coburn, E. Nazaretski, W. Xu, M. Ge, C. Longo, H. Xu, K. Gofron, Z. Yin, H. H. Chen, Y. Hwu, and W. K. Lee, "Design, characterization, and performance of a hard x-ray transmission microscope at the national synchrotron light source II 18-ID beamline," *Rev. Sci. Instrum.* **90**, 053701 (2019).
- ⁹M. Berglund, L. Rymell, and H. M. Hertz, "Compact water-window transmission X-ray microscopy," *J. Microsc.* **197**, 268–273 (2000).
- ¹⁰P. Russbueltd, D. Hoffmann, M. Höfer, J. Löhring, J. Luttmann, A. Meissner, J. Weitenberg, M. Traub, T. Sartorius, D. Esser, R. Wester, P. Loosen, and R. Poprawe, "Innoslab amplifiers," *IEEE J. Sel. Top. Quantum Electron.* **21**, 447–463 (2015).
- ¹¹D. Attwood and A. Sakdinawat, *Soft X-Rays and Extreme Ultraviolet Radiation* (Cambridge University Press, 2016).
- ¹²K. Thurner, F. P. Quacquarelli, P.-F. Braun, C. D. Savio, and K. Karrai, "Fiber-based distance sensing interferometry," *Appl. Opt.* **54**, 3051 (2015).